STED Microscopy

International Edition: DOI: 10.1002/anie.201511018
German Edition: DOI: 10.1002/ange.201511018

Fluorescent Rhodamines and Fluorogenic Carbopyronines for Super-Resolution STED Microscopy in Living Cells

Alexey N. Butkevich, Gyuzel Yu. Mitronova, Sven C. Sidenstein, Jessica L. Klocke, Dirk Kamin, Dirk N. H. Meineke, Elisa D'Este, Philip-Tobias Kraemer, Johann G. Danzl, Vladimir N. Belov,* and Stefan W. Hell**

Abstract: *A range of bright and photostable rhodamines and carbopyronines with absorption maxima in the range of $\lambda = 500$–630 nm were prepared, and enabled the specific labeling of cytoskeletal filaments using HaloTag technology followed by staining with 1 μM solutions of the dye–ligand conjugates. The synthesis, photophysical parameters, fluorogenic behavior, and structure–property relationships of the new dyes are discussed. Light microscopy with stimulated emission depletion (STED) provided one- and two-color images of living cells with an optical resolution of 40–60 nm.*

Fluorescent dyes are widely used as indispensable markers in biology-related optical microscopy.[1] The selective, sensitive, and stable imaging of cellular microstructure depends on the optimal combination of several chemical, biological, and physical factors. The availability and proper choice of fluorescent markers—fluorescent proteins (FPs) or synthetic fluorescent dyes—are key factors to the success of the entire labeling and imaging sequence. Owing to their superior brightness and photostability, synthetic dyes represent an attractive alternative to fluorescent proteins.

Herein, we introduce a set of cell-permeant fluorescent markers for living cells and apply them in one- and two-color super-resolution optical microscopy with stimulated emission depletion (STED).[2] For the specific labeling of intracellular targets in living cells, we used a well-established and robust procedure based on HaloTag fusion proteins.[3] In this technology, the protein of interest is genetically fused with an engineered enzyme (modified *Rhodococcus rhodochrous* dehalogenase), which is able to selectively and rapidly form a covalent bond with the substrate.

The variety of fluorescent probes applicable for the intracellular labeling of living cells is restricted owing to cell-permeability requirements. Several rhodamine dyes,[4] carbopyronines,[5] and silicon rhodamines (*SiR*)[6] are known to penetrate the outer plasma membranes of intact cells,[7] and methods for improving their brightness have recently been proposed.[1h] Unfortunately, the spectral variety of photostable fluorescent dyes suitable for intracellular targeting and super-resolution imaging in living cells is quite limited, and only few of them are commercially available (see the Supporting Information, Figure S1).

In commercial STED microscopes, three depletion regions are available: $\lambda = 592/595$ nm, 660 nm, and 765/775 nm.[8] Red (≥ 620 nm) or near-infrared (NIR; ≥ 750 nm) depletion lasers are advantageous as they cause less damage to biological objects and benefit from reduced autofluorescence, photobleaching, and light scattering. Therefore, the present study was focused on the design and evaluation of new cell-permeant fluorophores for STED microscopy with orange-red (618 nm) and NIR (775 nm) depletion lasers.

We learned empirically that cell-permeant probes are preferably electronically neutral (or zwitterionic with a short charge separation distance and zero net charge) and possess a compact structure, limited molecular mass ($M < 700$ Da), and several heteroatoms as hydrogen-bond donors and acceptors. Based on these criteria, we prepared several green-, yellow-, and red-emitting rhodamines, carbopyronines, and silicon rhodamines (Scheme 1). The spectral properties of these dyes are given in Table 1 and Figure S2. Only the 6′-carboxy isomers of the fluorophores have been shown to provide the successful labeling of proteins by means of HaloTag and SNAP-tag self-labeling techniques.[9] Therefore, we fixed the attachment of the HaloTag ligand to the 6′-position (or a topologically identical position) of the pendant aromatic ring and employed the original bis(oxyethylene) linker.[3]

The carbopyronines and Si-rhodamines **1f–k** were prepared from substituted anthrones or 10-silaanthrones (dibenzo[*b*,*e*]silin-10(5*H*)-ones) **2** as shown in Scheme 2. This modular approach allowed us to choose the tricyclic fragment of the fluorophore and the dicarboxylated aromatic ring independently. Carbopyronine **1e** was prepared from the corresponding carbofluorescein ditriflate[5f] by Buchwald–Hartwig amidation with BocNHMe[4d] (Boc = *tert*-butoxycarbonyl) followed by deprotection (see the Supporting Information for the synthetic method and analytical data). While

[*] Dr. A. N. Butkevich, Dr. G. Y. Mitronova, M. Sc. S. C. Sidenstein, B. Sc. J. L. Klocke, Dr. D. Kamin, M. Sc. D. N. H. Meineke, Dr. E. D'Este, Dr. P.-T. Kraemer, Dr. J. G. Danzl, Dr. V. N. Belov, Prof. Dr. S. W. Hell
Department of NanoBiophotonics
Max Planck Institute for Biophysical Chemistry
Am Fassberg 11, 37077 Göttingen (Germany)
E-mail: abutkev@gwdg.de
vbelov@gwdg.de
shell@gwdg.de
Homepage: http://www.mpibpc.gwdg.de/abteilungen/200/

Supporting information and ORCID(s) from the author(s) for this article are available on the WWW under http://dx.doi.org/10.1002/anie.201511018.

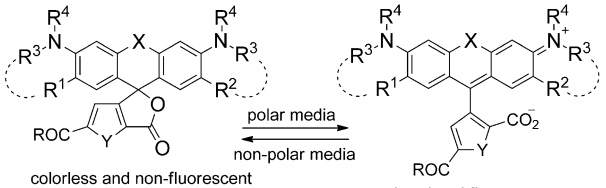

1a-k: R = OH; **1a-k**-Halo: R = NH[$(CH_2)_2O]_2(CH_2)_6$Cl

X = O, Y = CH=CH (rhodamines):
a) $R^1 = R^2 = R^3$ = H, $R^4 = F_3CCH_2$- (**1a**, *500R*);
b) $R^1 = R^2$ = F, R^3 = H, R^4 = Me (**1b**, *515R*);
c) $R^1 = R^2 = R^3$ = H, R^4 = Me (**1c**, *520R*);
d) R^1-R^3 = R^2-R^3 = -$C(CH_2OH)$=$CHCMe_2$-, R^4 = Me (**1d**, *580R*).
X = $C(CH_3)_2$, Y = CH=CH (carbopyronines):
e) $R^1 = R^2 = R^3$ = H, R^4 = Me (**1e**, *580CP*);
f) $R^1 = R^2$ = H, $R^3 = R^4$ = Me (**1f**, *610CP*);
g) R^1= H, R^2 = F, $R^3 = R^4$ = Me (**1g**, *620CP*);
h) $R^1 = R^2$ = F, $R^3 = R^4$ = Me (**1h**, *630CP*).
X = $Si(CH_3)_2$ (Si-rhodamines):
i) Y = CH=CH, $R^1 = R^2$ = H, $R^3 = R^4$ = Me (**1i**, *SiR*);
j) Y = S, $R^1 = R^2$ = H, $R^3 = R^4$ = Me (**1j**, *650SiR*);
k) Y = CH=CH, $R^1 = R^2$ = F, $R^3 = R^4$ = Me (**1k**, *670SiR*).

Scheme 1. Membrane-permeant fluorescent dyes for STED microscopy of living cells that are in equilibrium between non-fluorescent and fluorescent forms (for the spectral properties, see Table 1).

Table 1: Spectral properties of cell-permeant dyes in aqueous PBS buffer (pH 7.4) at room temperature; STED at $\lambda = 587$ (**1a**), 618 (**1b**,**c**), and 775 nm (**1d**–**k**).

Dye	Absorption λ_{max} [nm] (ε [M^{-1} cm^{-1}])	Emission λ_{max} [nm] (Φ_{fl})[a]	Brightness rel. to *SiR*[b]	$D_{0.5}$[c]	Fluorescence lifetime τ [ns]
500R (**1a**)	501 (88000)	523 (0.93)	2.15	32.5	4.2
515R (**1b**)	515 (56000)	543 (0.86)	1.26	19.6	4.1
520R (**1c**)	521 (52000)	546 (0.79)	1.08	7.5	4.0
580R (**1d**)	581 (58000)	607 (0.95)	1.45	< 5.6	3.9
580CP (**1e**)	582 (90000)	607 (0.69)	1.63	34.6	3.6
610CP (**1f**)	609 (100000)	634 (0.59)	1.55	36.4	3.1
620CP (**1g**)	617 (73000)	647 (0.17)	0.33	62.8	1.0
630CP (**1h**)	628 (6700)	660 (0.06)	0.01	72.7	0.4
SiR (**1i**)	645 (93000)	661 (0.41)	1 (ref.)	64.5	2.7
650SiR (**1j**)	650 (42000)	672 (0.36)	0.40	< 5.6	2.5
670SiR (**1k**)	670 (150)	696 (0.03)	0.0001	–	1.9[d]

[a] See the Supporting Information for details. [b] Brightness relative to *SiR*: $(\varepsilon \times \Phi_{fl})_{dye}/(\varepsilon \times \Phi_{fl})_{SiR}$. [c] See Figure 1 and the main text. [d] In methanol with 1% (v/v) of trifluoroacetic acid.

fluorination of the rhodamine tricyclic core led to small blue shifts of the absorption and emission bands (compare *515R* and *520R*), fluorination of the carbopyronine (**1g**,**h**) and Si-rhodamine (**1k**) cores resulted in dyes with red-shifted absorption and emission maxima, so that the new analogues are excitable at $\lambda = 600$–670 nm (Table 1). However, the emission quantum yields and fluorescence lifetimes of the fluorinated carbopyronines (**1g**,**h**) and Si-rhodamine dye **1k** were significantly reduced.

Fluorogenic behavior (a marked fluorescence intensity increase in response to an intracellular event of interest)[10] has recently been observed for the *SiR* dye **1i** bearing a HaloTag, SNAP-tag, or CLIP-tag ligand,[6h] and for *SiR*-based actin and tubulin probes.[6k] The emission of these

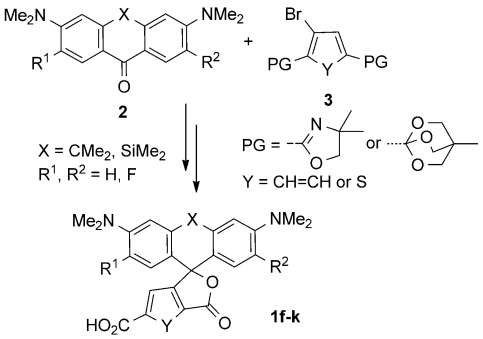

Scheme 2. General approach to the red-emitting dyes **1f**–**k** with a free carboxyl group for conjugation. PG = protecting group.

conjugates substantially increased upon binding to their target protein, whereas they emitted poorly in their free state (or bound to off-target proteins or hydrophobic structures) because the equilibrium was shifted to the non-fluorescent spirolactone form (Scheme 1). It was therefore of interest to correlate the fluorogenic behavior of the new dyes with their performance in live-cell imaging.

To evaluate the response of our dyes to the polarity of the medium, a series of absorption spectra were recorded in aqueous dioxane solutions with water contents from 10 to 100% and dielectric constants (D) from 5.6 to 78.3 (Figure 1).[6h] As expected, upon increasing the water content, the colorless spirolactone forms of all dyes underwent ring opening to the colored and fluorescent zwitterionic forms. Rhodamine dyes **1b**–**d** favor the zwitterionic form in all but the most non-polar solvent systems, whereas the carbopyronines **1e**–**h** and *SiR* **1i** exist predominantly in the lactone form in solutions with > 50% dioxane content ($D < 34.3$). For the *SiR* thiophene analogue (*650SiR*, **1j**),[11] cyclization into the colorless lactone form is impeded by the increase in angle strain upon formation of a five-membered lactone fused to a five-membered thiophene ring.

As a measure of the response of the dye to changes in solvent polarity, we defined $D_{0.5}$, the dielectric constant of a dioxane–water mixture at which the normalized absorption A/A_{max} (or extinction $\varepsilon/\varepsilon_{max}$) of the dye is equal to one half of the maximal value observed across the entire dioxane–water gradient (Figure 1). On this scale, low values of $D_{0.5}$ correspond to non-fluorogenic dyes (rhodamines *520R* and *580R* (**1c**,**d**) and the *SiR* thiophene analogue **1j**), whereas intermediate (20–40: fluorinated rhodamines and carbopyronines **1a**,**b**,**e**, and **f**) and high values of $D_{0.5}$ (60–70: **1g**, *SiR*)[13] indicate fluorogenic behavior. Dye **1k** ($D_{0.5} > 70$) exists predominantly in the colorless lactone form and will likely be too dark for imaging. As evident from Figure 1, fluorination of the fluorophore core (rhodamine **1b** vs. **1c** and carbopyronines **1g**,**h** vs. **1f**) or the introduction of *N*-trifluoroethyl groups (**1a**) favored lactone ring closure in more polar solvent systems. This effect can be explained by the destabilization of the positive charge at the C9 position of

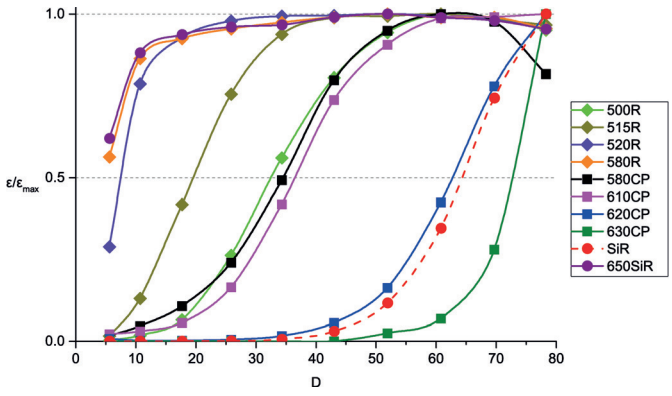

Figure 1. Normalized extinction, $\varepsilon/\varepsilon_{max}$, at λ_{max} of the dyes **1a–j** versus the dielectric constant, D, of dioxane–water mixtures. The $D_{0.5}$ values correspond to the intersection of interpolated graphs with a $\varepsilon/\varepsilon_{max} = 0.5$ line.[12] The absorbance of *580CP* (**1e**), *650SiR* (**1j**), and rhodamine dyes **1a–d** is non-monotonic at high D values owing to fluorophore–solvent interactions or dye aggregation.[6h]

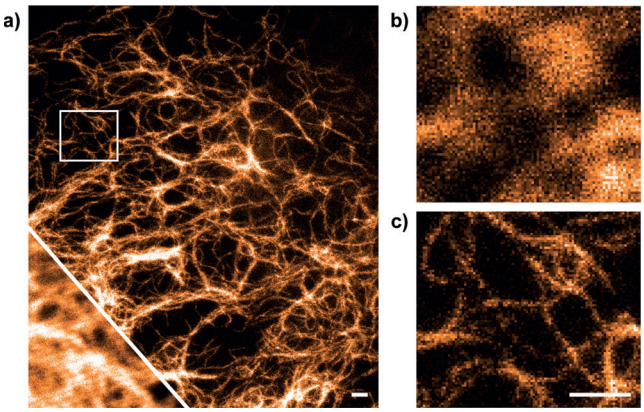

Figure 2. Confocal and STED images (raw data) of vimentin filaments in a living HeLa cell that expresses vimentin–HaloTag fusion protein after incubation with *520R* (**1c**-Halo; 1 μM for 20 min). a) STED image with the corresponding confocal data in the bottom left corner. b, c) Magnified views of the region marked in (a) of the confocal and STED images, respectively. Optical resolution ca. 40 nm (see Figure S9). Scale bars: 500 nm; excitation power: 1.6 μW; STED power: 14 mW; pixel dwell time: 20 μs; pixel size: 18 nm for the STED, 20 nm for the confocal image. Each line was scanned twice, and the counts were accumulated.

the xanthene, dihydroanthracene, or dihydrosilaanthracene. On the contrary, the replacement of *N*,*N*-dimethylamino (**1f**) with *N*-methylamino groups (**1e**) did not significantly affect $D_{0.5}$, which may reflect the comparatively small difference between the Hammett σ_p parameters for these substituents (−0.83 vs. −0.70).[14]

In agreement with this trend, fluorinated carbopyronines showed a significant fluorogenic response, comparable to that of *SiR*. A more than ten-fold increase in fluorescence intensity was observed upon covalent binding of **1g**,**h** to the HaloTag protein (Figure S3), whereas the conjugates of the rhodamine dyes **1b–d**-Halo, *610CP* (**1f**-Halo), and *650SiR* (**1j**-Halo) were much less responsive.

The magnitude of the response parallels the increase in fluorescence intensity of the tagged dyes **1a–k**-Halo, bound nonspecifically and reversibly to bovine serum albumin, upon addition of the anionic surfactant sodium dodecyl sulfate (SDS, see Figure S4), as shown previously for *SiR*.[6h,k] Interestingly, when the cationic surfactant cetyltrimethylammonium bromide was added instead of SDS, the fluorescence intensity decreased (Figure S4), suggesting that the fluorogenic response of the dyes **1g**, **1h**, and *SiR* may (at least partially) be due to interactions of the positively charged tricyclic fluorophore core with the local negative charges on the HaloTag protein surface in immediate proximity to its active site.

Three structurally similar green-emitting rhodamines, *500R*, *515R*,[4b] and *520R* (**1a–c**), were designed for STED wavelengths of 590 nm[8] and 618 nm (this work) applicable for the fluorescent proteins YFP and Citrine. For live-cell nanoscopy, we labeled vimentin filaments in living cells expressing a vimentin–HaloTag fusion protein (*515R*: HeLa, U2Os, Ptk2; *500R*, *520R*: HeLa; Figure 2). Upon incubation with 1 μM of the dye–ligand conjugates *500R*-, *515R*-, and *520R*-Halo for 20 min and washing for 10 min in dye-free cell culture medium, the cells exhibited bright and uniform staining of the vimentin fibers with virtually no nonspecific background fluorescence. STED microscopy with a 587 nm (**1a**) or 618 nm (**1b**,**c**) pulsed depletion laser afforded optical resolutions of approximately 40 nm for *500R* and *520R* and approximately 50 nm for *515R* in living samples (Figures S7–S9). The dyes *515R* and *520R* were found to be more photostable than Citrine under STED conditions (Figure S10), and the photostabilities increase in the order Citrine < *515R* < *520R*.

In the red spectral region (with a STED wavelength of 775 nm), the derivatives of rhodamine *580R* (**1d**-Halo), carbopyronines (**1e–h**-Halo), and Si-rhodamines (**1i–k**-Halo) were tested as fluorescent markers for the vimentin–HaloTag fusion protein. For three dyes (*580R*, *580CP*, and *610CP*; Figure 3), the confocal and STED images were bright and free from background fluorescence, and the staining was uniform. The optical resolution was ≤70 nm for *580CP*, ≤60 nm for *580R*, and approximately 50 nm for *610CP* (Figures S11–S13). The dyes *620CP* and *650SiR* gave more background (Figures S15, S16), whereas the difluorinated dyes *630CP* and *670SiR* produced insufficiently bright images.

The two dyes *580R* and *580CP* can be combined with *SiR*[6h,k] in two-color STED microscopy as all three can be depleted at $\lambda = 775$ nm with a single STED laser, ensuring perfect alignment of the two color channels.[4e] Whereas *SiR* is excited at $\lambda \approx 640$ nm, and its fluorescence is detected at 650–700 nm, *580R* and *580CP* can be excited at $\lambda \approx 560$ nm or 590 nm and detected at 605–625 nm, enabling clear color separation for *580R* (Figure S5) with low crosstalk between the channels. Figures 4 and S17 show two-color STED images of living HeLa cells (vimentin fibers labeled with *580R* or 580*CP*, respectively; tubulin labeled with a *SiR* tubulin probe).[6k] As evident from both Figures, a larger cross section for stimulated emission of the red-shifted dye at the STED wavelength results in higher optical resolution for the long-wavelength (*SiR*) channel. An independent choice of the STED power for each channel would improve the resolution

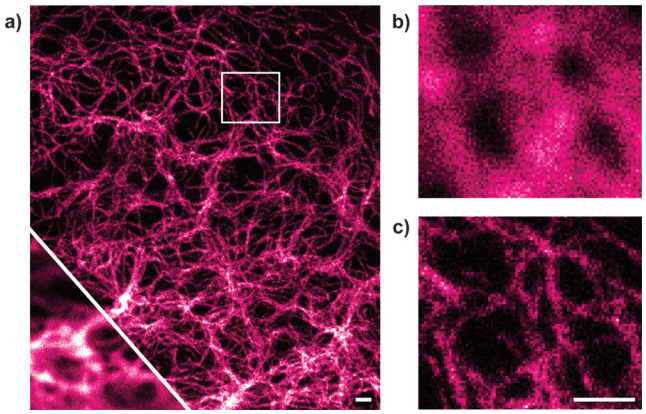

Figure 3. Confocal and STED images (raw data) of vimentin filaments in a living HeLa cell that expresses the vimentin–HaloTag fusion protein after incubation with *610CP* (**1f**-Halo; 1 μM for 20 min). a) STED image with the corresponding confocal data in the bottom left corner. b,c) Magnified views of the region marked in (a) of the confocal and STED images, respectively. Optical resolution ca. 50 nm (see Figure S13). Scale bars: 500 nm; pixel dwell time: 20 μs; pixel size: 20 nm for both the STED and the confocal image. Each line was scanned twice, and the counts were accumulated.

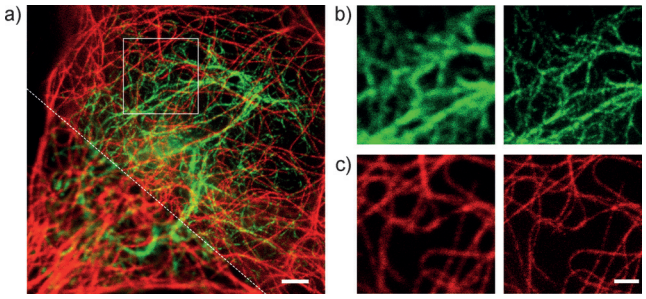

Figure 4. Two-color STED image (raw data) of vimentin (green) and tubulin (red) in a living HeLa cell. Vimentin filaments were labeled with *580R* applied as **1d**-Halo (1 μM) via the HaloTag fusion protein, whereas endogenous tubulin was directly labeled with the SiR tubulin probe[6k] (0.5 μM). a) STED image with the corresponding confocal image in the bottom left corner. b,c) Magnified views of the region marked in (a) of the confocal and STED image, respectively, of the two colors. Scale bars: 2 μm; pixel dwell time: 40 μs for the SiR tubulin channel (red), 20 μs for *580R* (green); pixel size: 20 nm for the STED and the confocal image. Color channels were recorded pixel by pixel; each line was scanned three times, and the counts were accumulated.

in the green channel and increase the signal intensity in the red channel.

In conclusion, the position of the equilibrium responsible for the fluorogenic properties of dyes **1a–k** (Scheme 1) can be represented by a $D_{0.5}$ value (Table 1), which can be explained in terms of electronic factors and predicted for future dye analogues. The fluorogenic behavior of a dye can be tuned by the introduction of fluorine atoms in the alkyl chains (e.g., *500R*), the fluorophore core (*515R*, *620CP*), or the pendant aromatic ring.[15] The principles of dye design exemplified in this study may enable the development of fluorogenic dyes of other classes (e.g. coumarins, rhodols, acridines, Ge-[6c] and P-rhodamines).[16] We expect that our fluorescent dyes will perform just as well, or even better, when used with SNAP- and CLIP-tags, as their recognition units are inherently more hydrophilic than the HaloTag ligand.

Even though fluorogenic properties are advantageous for fluorescent labels, the rhodamine derivatives **1a–d** showed no distinct correlation between their $D_{0.5}$ values and image quality, as all four dyes bound specifically and produced images with negligible background (Table 1). The excellent performance of the dye *580R* in live-cell imaging despite its bulky and rigid polycyclic rhodamine core suggests that the hydroxylation of a fluorophore is a valuable tactic for rendering the dye hydrophilic, highly polar, and soluble in aqueous buffers without compromising its cell permeability.

The choice of fluorescent markers for live-cell nanoscopy will often be guided by the available instrumentation. The green-emitting rhodamines *500R* (**1a**), *515R* (**1b**), and *520R* (**1c**) performed exceptionally well with depletion lasers at 587 nm (**1a**) and 618 nm (**1b**,**c**). Dye *520R* is superior both in terms of attainable optical resolution and photostability in repeated imaging, making it potentially suitable for the time-lapse nanoscopy of dynamic biological processes. Taking into account that in STED microscopy, green/yellow FPs clearly outperform their red counterparts, the new synthetic dyes are advantageous over FPs in terms of their imaging performance in all spectral regions. With depletion at 775 nm, both rhodamine *580R* (**1d**) as well as the carbopyronines *580CP* and *610CP* (**1e**,**f**) performed well in live-cell imaging. As longer depletion wavelengths offer the advantage of diminished interactions with biological matter, the combination of *SiR* with *580R* or *580CP* dyes enables high-quality two-color live-cell nanoscale imaging and will be a natural choice for the most widely used 775 nm STED laser.

Acknowledgements

We thank Prof. Y. Okada (RIKEN Quantitative Biology Center, Osaka, Japan) for the gift of β-tubulin-Halo plasmid, T. Gilat and Dr. E. Rothermel (MPIBPC, Göttingen, Germany) for cell culture and transfection, M. Pulst, J. Bienert (MPIBPC), Dr. M. John, Dr. H. Frauendorf, and co-workers (Institut für Organische und Biomolekulare Chemie, Georg-August-Universität, Göttingen, Germany) for UV/Vis, NMR, and ESI-MS spectra, Prof. M. L. Bossi (University of Buenos-Aires, Argentina) for measuring fluorescence lifetimes, and Dr. S. Vos and Prof. P. Cramer (MPIBPC) for access to a Tecan microplate reader. S.W.H. acknowledges a grant from the Bundesministerium für Bildung und Forschung (BMBF 513) within the program "Optische Technologien für Biowissenschaften und Gesundheit" (FKZ 13N11066). J.G.D. was supported by funds from the People Programme (Marie Curie Actions) of the European Union's Seventh Framework Programme (FP7/2007–2013; REA grant agreement PIEF-GA-2011-299283).

Keywords: carbopyronines · fluorescence · living cells · optical microscopy · rhodamines

How to cite: *Angew. Chem. Int. Ed.* **2016**, *55*, 3290–3294
Angew. Chem. **2016**, *128*, 3350–3355

[1] a) M. Fernández-Suárez, A. Y. Ting, *Nat. Rev. Mol. Cell Biol.* **2008**, *9*, 929 – 943; b) M. S. T. Gonçalves, *Chem. Rev.* **2009**, *109*, 190 – 212; c) L. D. Lavis, R. T. Raines, *ACS Chem. Biol.* **2014**, *9*, 855 – 866; d) K. Umezawa, D. Citterio, K. Suzuki, *Anal. Sci.* **2014**, *30*, 327 – 349; e) S. van de Linde, M. Sauer, *Chem. Soc. Rev.* **2014**, *43*, 1076 – 1087; f) T. J. Chozinski, L. A. Gagnon, J. C. Vaughan, *FEBS Lett.* **2014**, *588*, 3603 – 3612; g) A. G. Godin, B. Lounis, L. Cognet, *Biophys. J.* **2014**, *107*, 1777 – 1784; h) J. B. Grimm, B. P. English, J. Chen, J. P. Slaughter, Z. Zhang, A. Revyakin, R. Patel, J. J. Macklin, D. Normanno, R. H. Singer, T. Lionnet, L. D. Lavis, *Nat. Methods* **2015**, *12*, 244 – 250.

[2] a) C. Eggeling, S. W. Hell, *STED Fluorescence Nanoscopy*, *Springer Ser. in Fluorescence* (Eds.: P. Tinnefeld, C. Eggeling, S. W. Hell), Springer, Berlin-Heidelberg, **2015**, pp. 4 – 25; b) "STED Microscopy": T. J. Gould, P. A. Pellett, J. Bewersdorf in *Fluorescence Microscopy*: *from Principles to Biological Applications*, Wiley-VCH, Weinheim, **2013**, pp. 375 – 392.

[3] a) G. V. Los, L. P. Encell, M. G. McDougall, D. D. Hartzell, N. Karassina, C. Zimprich, M. G. Wood, R. Learish, R. F. Ohana, M. Urh, D. Simpson, J. Mendez, K. Zimmerman, P. Otto, G. Vidugiris, J. Zhu, A. Darzins, D. H. Klaubert, R. F. Bulleit, K. V. Wood, *ACS Chem. Biol.* **2008**, *3*, 373 – 382; b) http://www.promegaconnections.com/tag/halotag.

[4] a) M. Beija, C. A. M. Afonso, J. M. G. Martinho, *Chem. Soc. Rev.* **2009**, *38*, 2410 – 2433; b) G. Y. Mitronova, V. N. Belov, M. L. Bossi, C. A. Wurm, L. Meyer, R. Medda, G. Moneron, S. Bretschneider, C. Eggeling, S. Jakobs, S. W. Hell, *Chem. Eur. J.* **2010**, *16*, 4477 – 4488; c) V. N. Belov, C. A. Wurm, V. P. Boyarskiy, S. Jakobs, S. W. Hell, *Angew. Chem. Int. Ed.* **2010**, *49*, 3520 – 3523; *Angew. Chem.* **2010**, *122*, 3598 – 3602; d) J. B. Grimm, L. D. Lavis, *Org. Lett.* **2011**, *13*, 6354 – 6357; e) K. Kolmakov, C. A. Wurm, D. N. H. Meineke, F. Göttfert, V. P. Boyarskiy, V. N. Belov, S. W. Hell, *Chem. Eur. J.* **2014**, *20*, 146 – 157.

[5] a) C. Aaron, C. C. Barker, *J. Chem. Soc. B* **1971**, 319 – 324; b) J. Arden-Jacob, J. Frantzeskos, N. U. Kemnitzer, A. Zilles, K.-H. Drexhage, *Spectrochim. Acta Part A* **2001**, *57*, 2271 – 2283; c) R. O'Neill, P. V. Fischer (Guava Tech. Inc.), WO 2004/003510 A2; d) K.-H. Drexhage, J. Arden-Jacob, J. Frantzeskos, A. Zilles, US 6828159 B1; e) K. Kolmakov, V. N. Belov, C. A. Wurm, B. Harke, M. Leutenegger, C. Eggeling, S. W. Hell, *Eur. J. Org. Chem.* **2010**, 3593 – 3610; f) J. B. Grimm, A. J. Sung, W. R. Legant, P. Hulamm, S. M. Matlosz, E. Betzig, L. D. Lavis, *ACS Chem. Biol.* **2013**, *8*, 1303 – 1310.

[6] a) M. Fu, Y. Xiao, X. Qian, D. Zhao, Y. Xu, *Chem. Commun.* **2008**, 1780 – 1782; b) Y. Koide, Y. Urano, K. Hanaoka, W. Piao, M. Kusakabe, N. Saito, T. Terai, T. Okabe, T. Nagano, *J. Am. Chem. Soc.* **2012**, *134*, 5029 – 5031; c) Y. Koide, Y. Urano, K. Hanaoka, T. Terai, T. Nagano, *ACS Chem. Biol.* **2011**, *6*, 600 – 608; d) T. E. McCann, N. Kosaka, Y. Koide, M. Mitsunaga, P. L. Choyke, T. Nagano, Y. Urano, H. Kobayashi, *Bioconjugate Chem.* **2011**, *22*, 2531 – 2538; e) T. Pastierik, P. Šebej, J. Medalová, P. Štacko, P. Klán, *J. Org. Chem.* **2014**, *79*, 3374 – 3382; f) P. Shieh, M. S. Siegrist, A. J. Cullen, C. R. Bertozzi, *Proc. Natl. Acad. Sci. USA* **2014**, *111*, 5456 – 5461; g) T. Wang, Q.-J. Zhao, H.-G. Hu, S.-C. Yu, X. Liu, L. Liu, Q.-Y. Wu, *Chem. Commun.* **2012**, *48*, 8781 – 8783; h) G. Lukinavičius, K. Umezawa, N. Olivier, A. Honigmann, G. Yang, T. Plass, V. Mueller, L. Reymond, I. R. Corrêa, Jr., Z.-G. Luo, C. Schultz, E. A. Lemke, P. Heppenstall, C. Eggeling, S. Manley, K. Johnsson, *Nat. Chem.* **2013**, *5*, 132 – 139; i) E. Kim, K. S. Yang, R. J. Giedt, R. Weissleder, *Chem. Commun.* **2014**, *50*, 4504 – 4507; j) B. Wang, X. Chai, W. Zhu, T. Wang, Q. Wu, *Chem. Commun.* **2014**, *50*, 14374 – 14377; k) G. Lukinavičius, L. Reymond, E. D'Este, A. Masharina, F. Göttfert, H. Ta, A. Günther, M. Fournier, S. Rizzo, H. Waldmann, C. Blaukopf, C. Sommer, D. W. Gerlich, H.-D. Arndt, S. W. Hell, K. Johnsson, *Nat. Methods* **2014**, *11*, 731 – 733; l) P. Horváth, P. Šebej, T. Šolomek, P. Klán, *J. Org. Chem.* **2015**, *80*, 1299 – 1311; m) Y. Kushida, T. Nagano, K. Hanaoka, *Analyst* **2015**, *140*, 685 – 695.

[7] The structures of the cell-permeable fluorescent dyes and their HaloTag ligand derivatives, available from Promega Corp. (AMCA, Rhodamine 110, TMR, and di-O-acetylated derivatives of fluorescein and Oregon Green) and Spirochrom (*SiR*), are given in Figure S1.

[8] Abberior Instruments GmbH offers STED microscopes with pulsed 595 nm and 775 nm depletion lasers; Leica Microsystems: 592 nm (gated; CW), 660 nm (gated; CW), and 775 nm (pulsed) depletion lasers; PicoQuant GmbH: 765 nm depletion laser.

[9] a) F. Stagge, G. Y. Mitronova, V. N. Belov, C. A. Wurm, S. Jakobs, *PLoS One* **2013**, *8*, e78745; b) I. R. Corrêa, Jr., B. Baker, A. Zhang, L. Sun, C. R. Provost, G. Lukinavičius, L. Reymond, K. Johnsson, M.-Q. Xu, *Curr. Pharm. Des.* **2013**, *19*, 5414 – 5420.

[10] a) A. Nadler, C. Schultz, *Angew. Chem. Int. Ed.* **2013**, *52*, 2408 – 2410; *Angew. Chem.* **2013**, *125*, 2466 – 2469; b) Y. Hori, K. Kikuchi, *Curr. Opin. Chem. Biol.* **2013**, *17*, 644 – 650; c) Y. Chen, K. Tsao, J. W. Keillor, *Can. J. Chem.* **2015**, *93*, 389 – 398.

[11] K. Groves, R. Buff (Visen Medical, Inc.), WO 2014/144793 A1.

[12] Processed with Origin 9.1 software using modified Bézier curves; see http://www.originlab.com/doc/Origin-Help/PD-Dialog-Line-Tab for the explanation of the algorithm. More rigorously, the $D_{0.5}$ value for a dye can be obtained by solving the equation $d^2(\varepsilon/\varepsilon_{max})/dD^2 = 0$.

[13] The value for *SiR* measured by us ($D_{0.5} = 64.5$) is higher than the value ($D_{0.5} \approx 30$) estimated from the plot (Figure 1b) in Ref. [6h].

[14] C. Hansch, A. Leo, R. W. Taft, *Chem. Rev.* **1991**, *91*, 165 – 195.

[15] K. Kolmakov, E. Hebisch, T. Wolfram, L. A. Nordwig, C. A. Wurm, H. Ta, V. Westphal, V. N. Belov, S. W. Hell, *Chem. Eur. J.* **2015**, *21*, 13344 – 13356.

[16] X. Chai, X. Cui, B. Wang, F. Yang, Y. Cai, Q. Wu, T. Wang, *Chem. Eur. J.* **2015**, *21*, 16754 – 16758.

Received: November 26, 2015
Published online: February 4, 2016

